Available online at www.sciencedirect.com
ScienceDirect
Remote Sensing of Environment 107 (2007) 65–80
Remote Sensing of Environment
www.elsevier.com/locate/rse

Application of satellite and ground-based data to investigate the UV radiative effects of Australian aerosols

Olga V. Kalashnikova [a,*], Franklin P. Mills [b], Annmarie Eldering [a], Don Anderson [c]

[a] Jet Propulsion Laboratory, California Institute of Technology, Pasadena, CA, USA
[b] Centre for Resource and Environmental Studies, Australian National University, Canberra, ACT, Australia
[c] Bureau of Meteorology, Melbourne, VIC, Australia

Received 13 February 2006; received in revised form 20 June 2006; accepted 16 July 2006

Abstract

An understanding of the effect of aerosols on biologically- and photochemically-active UV radiation reaching the Earth's surface is important for many ongoing climate, biophysical, and air pollution studies. In particular, estimates of the UV characteristics of the most common Australian aerosols will be valuable inputs to UV Index forecasts, air quality studies, and assessments of the impact of regional environmental changes. By analyzing climatological distributions of Australian aerosols we have identified sites where co-located ground-based UV-B and ozone measurements were available during episodes of relatively high aerosol activity. Since at least June 2003, surface UV global irradiance spectra (285–450 nm) have been measured routinely at Darwin and Alice Springs in Australia by the Australian Bureau of Meteorology (BoM). Using co-located sunphotometer measurements at Darwin and Alice Springs, we identified several episodes of relatively high aerosol activity. Aerosol air mass types were analyzed from sunphotometer-derived angstrom parameter, MODIS fire maps and MISR aerosol property retrievals. To assess aerosol effects we compared the measured UV irradiances for aerosol-loaded and clear-sky conditions with each other and with irradiances simulated using the libRadtran radiative transfer model for aerosol-free conditions. We found that for otherwise similar atmospheric conditions, smoke aerosols over Darwin reduced the surface UV irradiance by as much as 40–50% at 290–300 nm and 20–25% at 320–400 nm near active fires (aerosol optical depth, AOD, at 500 nm ~ 0.6). Downwind of fires, the smoke aerosols over Darwin reduced the surface irradiance by 15–25% at 290–300 nm and ~ 10% at 320–350 nm (AOD at 500 nm ~ 0.2). The effect of smoke increased with decrease of wavelength and is strongest in the UV-B. The aerosol attenuation factors calculated for the selected cases suggest smoke over Darwin has an effect on surface 340–380 nm irradiances that is comparable to that produced by smoke over Sub-Saharan Africa. Dust activity was very low at Alice Springs during 2004, therefore we were not able to identify strong dust events to fully assess the UV effect of dust. For the cases studied, smoke aerosols seem to produce a stronger reduction in surface UV irradiances than dust aerosols.

Keywords: Australian aerosols; UV surface irradiances; MISR; MODIS

1. Introduction

Australia has comparatively high levels of surface UV radiation. The annual mean daily UV Index (UVI) derived from broadband radiometer measurements at Alice Springs and Darwin in 1996–2000 was 9.0 and 10.1, respectively, while the annual mean daily UVI at UK sites was no more than 2.4 (Gies et al., 2004). The UVI describes the biologically-effective solar radiation reaching the Earth's surface at a location. It is determined by weighting the incident solar radiation at the Earth's surface with the erythemal response of human skin at 280–400 nm and then summing over this wavelength range to derive a total effect. One UVI unit is equivalent to biologically-effective solar UV radiation of 0.025 W m^{-2} effective (Gies et al., 2004). The UVI can be reported as a continuous measure but the most common value reported is the maximum UVI for each day. A UVI of 3–5 is considered "moderate", a UVI of 8–10 is "very high", and a UVI greater than 10 is "extreme" (WHO, 2002). The high levels of surface UV radiation in Australia occur mainly because Australia is located close to the equator and generally has clear, pollution-free atmospheric conditions.

* Corresponding author. Tel.: +1 818 393 0469.
E-mail address: Olga.V.Kalashnikova@jpl.nasa.gov (O.V. Kalashnikova).

0034-4257/$ - see front matter © 2006 Elsevier Inc. All rights reserved.
doi:10.1016/j.rse.2006.07.025

Moreover, solar radiation is ~ 7–10% more intense in the Southern Hemisphere at summer solstice compared to the Northern Hemisphere because southern summer solstice occurs at perihelion. Australia can also be affected by transport of air from Antarctica that has been depleted in ozone, particularly in southern spring to summer. Public health officials raise concerns over exposure to both UV-A (315–400 nm) and UV-B (280–315 nm) in Australia. With a predominately-fair-skin population and an outdoor lifestyle, the resulting skin-cancer rates are among the highest in the world (Slevin et al., 2000). An increase in the surface UV irradiance could also harm terrestrial and oceanic vegetation, degrade man-made objects, change the chemistry of the lower atmosphere (e.g. photochemical smog formation), and alter plant biochemical cycles. Consequently, understanding the factors that affect Australian surface UV radiation levels has significant scientific and social interest.

Surface UV irradiance primarily is controlled by the exoatmospheric solar radiation, surface elevation, solar zenith angle, surface cover, ozone, aerosols, and clouds. Changes in the surface UV irradiance due to changes in the exoatmospheric intensity, surface elevation, and solar zenith angle are predictable, and the relation between stratospheric ozone and surface UV irradiance is well established (Madronich et al., 1998). Less is known about the effects of surface type but the reflectivity of most land surfaces, excluding snow or ice covered areas, is low. The effects of aerosols and clouds on surface UV irradiances, however, are significant but are often poorly constrained and the direct effects can be magnified by the interaction of multiply-scattered solar UV with tropospheric ozone. The magnitude of the net aerosol effect can be large (over certain parts of the Earth, aerosols can reduce the UV flux at the surface by more than 50% (Krotkov et al., 1998)) and is highly variable, depending on the number of particles and their physical and chemical properties. Usually particles tend to reduce the surface UV irradiance, however, scattering by non-UV-absorbing particles (background aerosols) can increase the UV exposure on non-horizontal surfaces due to additional scattering from low angles (Dickerson et al., 1997). Lui et al. (1991) estimated that anthropogenic sulfate aerosols have decreased surface UV-B irradiances by 5 to 18%; Kylling et al. (1998) found that surface UV irradiances measured at two sites in Greece under non-cloudy conditions were reduced compared to aerosol-free conditions by 5 to 35%, depending on aerosol optical depth (AOD) and single-scattering albedo. Very few comparative studies have been done on the effects of different type of aerosols on UV radiation. Balis et al. (2004) have shown from a co-located Raman lidar system and spectral UV-B irradiance measurements that for the same AOD and for the same ozone column, surface UV-B irradiances may differ by up to 10%, which was attributed to differences in aerosol type. In addition, some modeling studies (Diaz et al., 2000) have suggested that aerosol vertical (height) distribution can also affect surface UV irradiances by 2–5% for optical depth ~ 0.5 at visible wavelengths. Due to the combined involvement of different aerosol parameters in controlling UV levels, it is difficult to determine accurately the role of each parameter. Nevertheless, it is important to understand the effects that aerosols have on surface UV irradiances. Australia is an ideal place to study the effects on surface UV irradiances due to two types of naturally-occurring UV-absorbing aerosols – smoke and mineral dust – because of Australia's occasional high atmospheric loadings of each of these two types of aerosols, Australia's generally-clear-sky conditions, and Australia's very low loading of urban aerosols (e.g., pollution, including soot), which could confound efforts to isolate the effects that natural smoke and mineral dust can have on surface UV irradiances.

In this paper we study the spectrally-resolved effects of two types of UV-absorbing aerosols affecting the Australian continent: dust and smoke. We also investigate whether the aerosol UV spectral effects change with distance downwind from the aerosol source region because particle properties may change during transport and aging (Torres et al., 1998). As noted above, the effects of aerosols on surface UV irradiances have been studied in many parts of the northern hemisphere, but information on the impact of Australian aerosols is much more limited. The UV spectra reported here are among the first data from an Australian Bureau of Meteorology (BoM) program that was initiated recently to measure spectrally-resolved UV irradiances at selected sites around Australia. A small dust source was identified in central Australia based on initial studies using the TOMS Aerosol Index (AI) (Herman et al., 1997), and several smaller Australian dust sources were identified in later studies based on the TOMS AI (Prospero et al., 2002). The TOMS AI also has been used in combination with ground-based sunphotometer measurements at visible wavelengths to study smoke from biomass burning in northern Australia (O'Brien & Mitchell, 2003), and airborne measurements and samples have been used to characterize smoke from biomass burning over northern Australia (Gras et al., 1999). None of these studies, however, has examined the effects of dust or smoke over Australia on the spectrally-resolved UV surface irradiances. The present study gives an initial estimate of how Australian smoke and mineral dust can affect surface UV irradiances.

Existing climatologies for Australian aerosols based on historical fire activity and data from the TOMS Aerosol Index were surveyed, Section 2, to confirm that the two sites (Darwin and Alice Springs) at which ground-based UV spectra have been measured regularly were good candidates for further study. A climatology for AOD and Angstrom parameter (446–867 nm) in 2004 based on MISR data was used to examine conditions during the first full calendar year for which UV spectra from both ground stations were available. The most direct determination that we could make of the spectrally-resolved effects of the two selected aerosol types was by comparing ground-based UV spectra from days on which the overhead aerosol loading was significant to spectra from days on which the aerosol loading was as small as possible. Specific dates for study were selected by examining sunphotometer data (Mitchell & Forgan, 2003) collected at each site and finding dates when sunphotometer data, UV spectrometer data, and satellite data (MISR and/or MODIS) were all available. This combination of data provides temporal context at the local site through the sunphotometer and UV spectrometer data and spatial context at the regional scale from the satellite data. The contextual information from the satellite data included the distance each measurement site was

from likely source region(s) for the cases with significant loadings of smoke aerosols. The satellite data were also an independent source for AOD and aerosol type (Angstrom parameter) information. We used daily average ozone column data from the BoM Dobson spectrophotometer at Darwin and from the Total Ozone Mapping Spectrometer (TOMS) for Alice Springs, AOD data from a CSIRO Aerosol Ground Station Network (AGSNet) sunphotometer at Darwin and from a BoM sunphotometer at Alice Springs, and spectrally-resolved UV surface irradiance data from BoM spectroradiometers at these two sites. The CSIRO sunphotometer data from Darwin for January to September 2004 were obtained via the Aerosol Robotic Network (AERONET) data distribution system. The CSIRO sunphotometer data from Darwin for October to November 2004 were obtained from Dr. Ross Mitchell. The BoM sunphotometer data from Alice Springs were obtained from Dr. Bruce Forgan.

In Section 2 we summarize the climatology for Australian aerosols based on a survey of recent articles and maps for 2004 of monthly mean AOD and Angstrom parameter derived from MISR data. We describe the BoM spectroradiometer instrument and our modeling approach in Sections 3 and 4, respectively. We then discuss selection of cases and present the results from our analysis of UV aerosol effects at Darwin and Alice Springs in Sections 5 and 6, respectively. Conclusions and some comparisons with the Northern Hemisphere results are summarized in Section 7.

2. Assessment of aerosol climatology in Australia

Australia in general has very low aerosol loadings compared to other continents and is mostly affected by smoke from controlled (planned) fires in the northern part of Australia (Craig et al., 2002) and by occasional dust outbreaks in the central to southern Australia (Prospero et al., 2002). Fig. 1 shows a climatology for seasonal fire activity and dust storms. This figure demonstrates that fires occur most commonly in northern Australia in winter and spring, which is the dry season for this region, while in southern Australia fires are most common in summer. A study based on fire hot spots observed via NOAA AVHRR imagery in April 1998 to March 2000 (Craig et al., 2002) observed a similar temporal pattern in the fire season and presented the spatial distribution of fire hot spots on annual and seasonal bases. The annual fire density (number of fires per unit area) was greatest in the area near Darwin. Queensland (east and north of the Great Dividing Range) and northern Western Australia also had annual high fire densities. The area near Darwin had high fire densities in autumn, winter, and spring. The far north of Queensland had high fire densities in winter and spring, while northeast and east Queensland had high fire densities in winter, spring, and summer. Southwest Western Australia and the southeastern agricultural lands (in New South Wales and Victoria) had high fire densities in summer and autumn. The remainder of Western Australia had high fire densities in spring and summer.

The characterization of dust sources with the TOMS Absorbing Aerosol Index (Herman et al., 1997; Prospero et al., 2002; Torres et al., 1998) indicates persistent dust activity in the interior of Australia. These publications attribute the source for this dust to be the great Artesian Basin, which feeds Lake Eyre, but O'Brien and Mitchell (2003) suggest the sources are the Simpson and Strzelecki deserts, which are the most active dust sources on the Australian continent (Middleton, 1984). A number of studies indicate that dust activity starts in austral spring, usually September to October, reaches a maximum in December to February (i.e. austral summer), and is usually over by May (Prospero et al., 2002; Shao & Leslie, 1997).

From this seasonal assessment of Australian dust and smoke activity we chose for this study two sites in Australia: Darwin – a smoky site (12.28 S, 130.51 E) – and Alice Springs — a dusty site (23.42 S, 133.53 E), where surface UV spectra (285–450 nm) have been measured routinely by the BoM since the later part of 2003. Darwin is located in northern Australia, has very low background aerosol loadings, and is affected by smoke during the local fire season (September to November). Alice Springs is located in central Australia near dust sources that become active during the Australian summer (December–March).

To assess the climatology of aerosols during 2004 we used the monthly-average Level 3 AOD (558 nm green band) and Angstrom parameter (446–867 nm) products from the Multi-angle Imaging SpectroRadiometer (MISR). MISR (launched on Terra in 1999) is a multi-angle (9 view) imaging instrument operating in four spectral bands centered at 446, 558, 672, and 867 nm (Diner et al., 1998). The fore-aft-nadir cameras acquire images with view angles, relative to the Earth's surface, at 0°, 26°, 46°, 60°, and 70°. In its global observing mode, the data in all bands of the nadir camera and the red band data of all of the off-nadir cameras are down-linked at full spatial resolution, 275 m. All other channels are averaged on-board to a resolution of 1100 m. The swath width is about 380 km, and global coverage is obtained every 9 days. MISR data are archived at the NASA Langley Atmospheric Sciences Data Center (ASDC). MISR's combination of multi-spectral and multi-angle data, which observe scattering angles from about 60° to 160° in mid-latitudes, allows retrievals of a combination of column-average particle size, shape, and single-scattering albedo (SSA) in addition to AOD and Angstrom parameter over both land and ocean (Diner et al., 1999; Kahn et al., 1998). Currently the only mid-visible AOD product was formally validated (Kahn et al., 2005). We are using this product to access spatial AOD coverage. In an addition, we are using Angstrom exponent product that, though not formally validated, provides an indication of differences between different air mass types and gives a guideline for particle property spatial coverage analysis.

The MISR monthly average Level-3 AOD product for April 2004 (Fig. 2) shows very low aerosol activity over Australia in April with AOD < 0.1. The MISR monthly average Level-3 AOD products for September to November 2004 (Fig. 3 left) show moderate to high values for AOD over northern Australia starting in September with maximum activity in November. Both AOD and Angstrom parameter over northern Australia show seasonality, with extended periods of low Angstrom parameter during the wet season (December–January) (Fig. 4 right) caused by the dominance of large particles, while periods

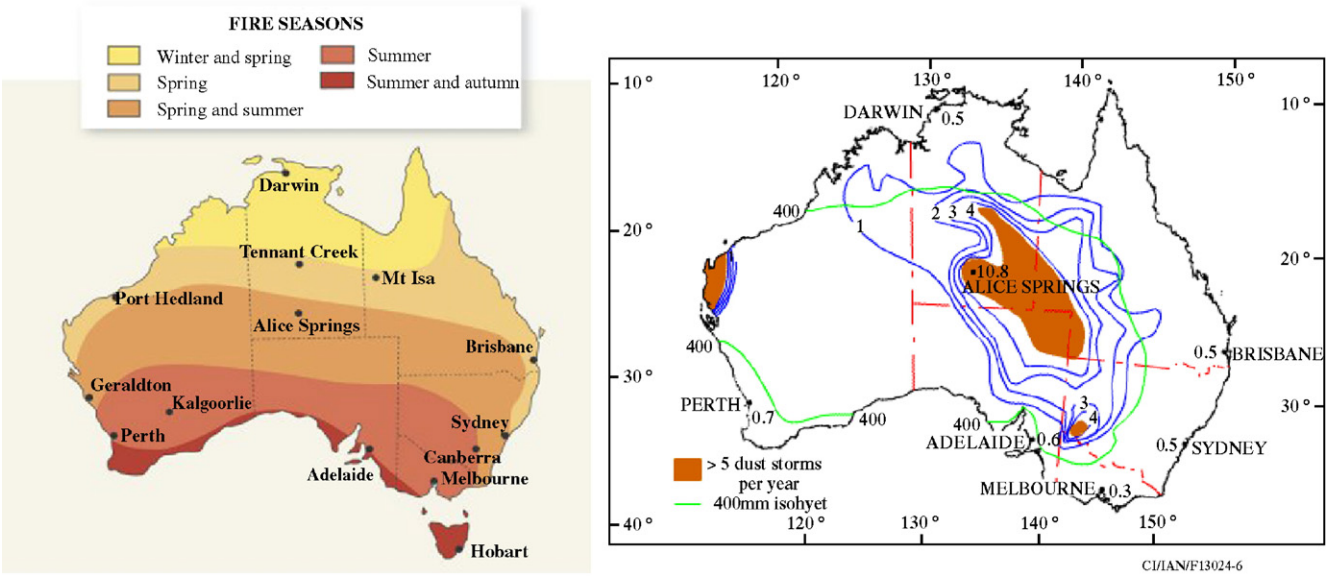

Fig. 1. Climatological distributions of fire seasons and dust activity over Australia. Original sources are BoM (2003) and Sqires (2004).

of high Angstrom parameter are associated with the peak of the burning season in September–November (Fig. 3 right), when small smoke particles dominate. A cloud screening algorithm has been applied to the MISR data prior to generating the Level-3 AOD and Angstrom parameter products, but it is possible that some of the low Angstrom parameters during the wet season are due to thin, spatially-uniform cirrus cloud, for which screening is problematic. MISR sensitivity studies indicate MISR-derived aerosol properties are less reliable if the AOD is <0.1 (Kahn et al., 2001, 1997).

The seasonality in AOD retrieved from MISR data agrees with the seasonality derived from sunphotometer observations at Darwin and Alice Springs. Fig. 5 shows the daily-averaged AOD derived from BoM sunphotometer measurements and indicates there was a peak of aerosol activity in November 2004 at Darwin and moderate to high aerosol loadings in January, November, and December 2004 at Alice Springs.

3. BoM spectroradiometer description

The spectrally-resolved UV data we used for our study were obtained by the BoM using Bentham spectroradiometers which began operating at Alice Springs and Darwin in May and June 2003, respectively (Fig. 6).

The spectroradiometers were supplied by the National Institute of Water and Atmosphere (NIWA) in New Zealand (Wuttke et al., 2006) and were modified for use at Alice Springs and Darwin. The spectroradiometers are based around a Bentham 300 mm focal length double monochromator with a 3600 line per mm diffraction grating. The entrance optic

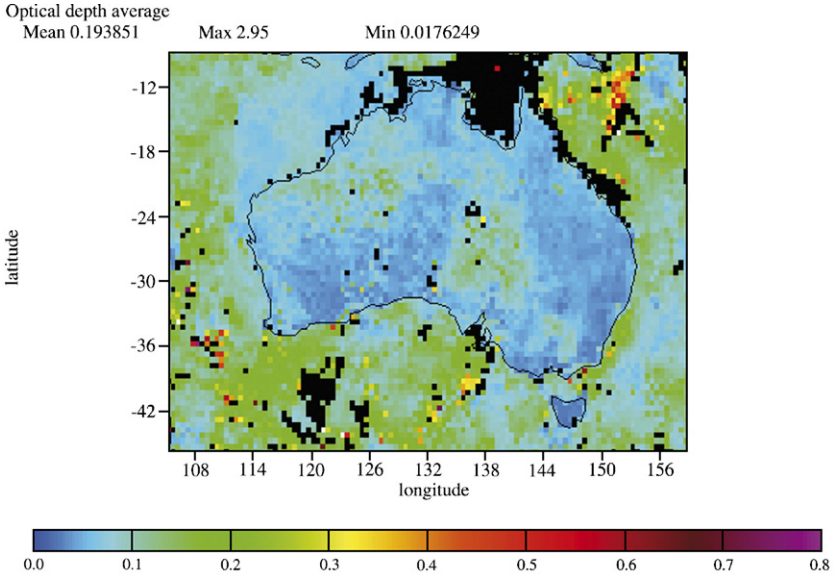

Fig. 2. MISR monthly aerosol climatology: monthly-averaged aerosol optical depth (green band AOD) product, April 2004.

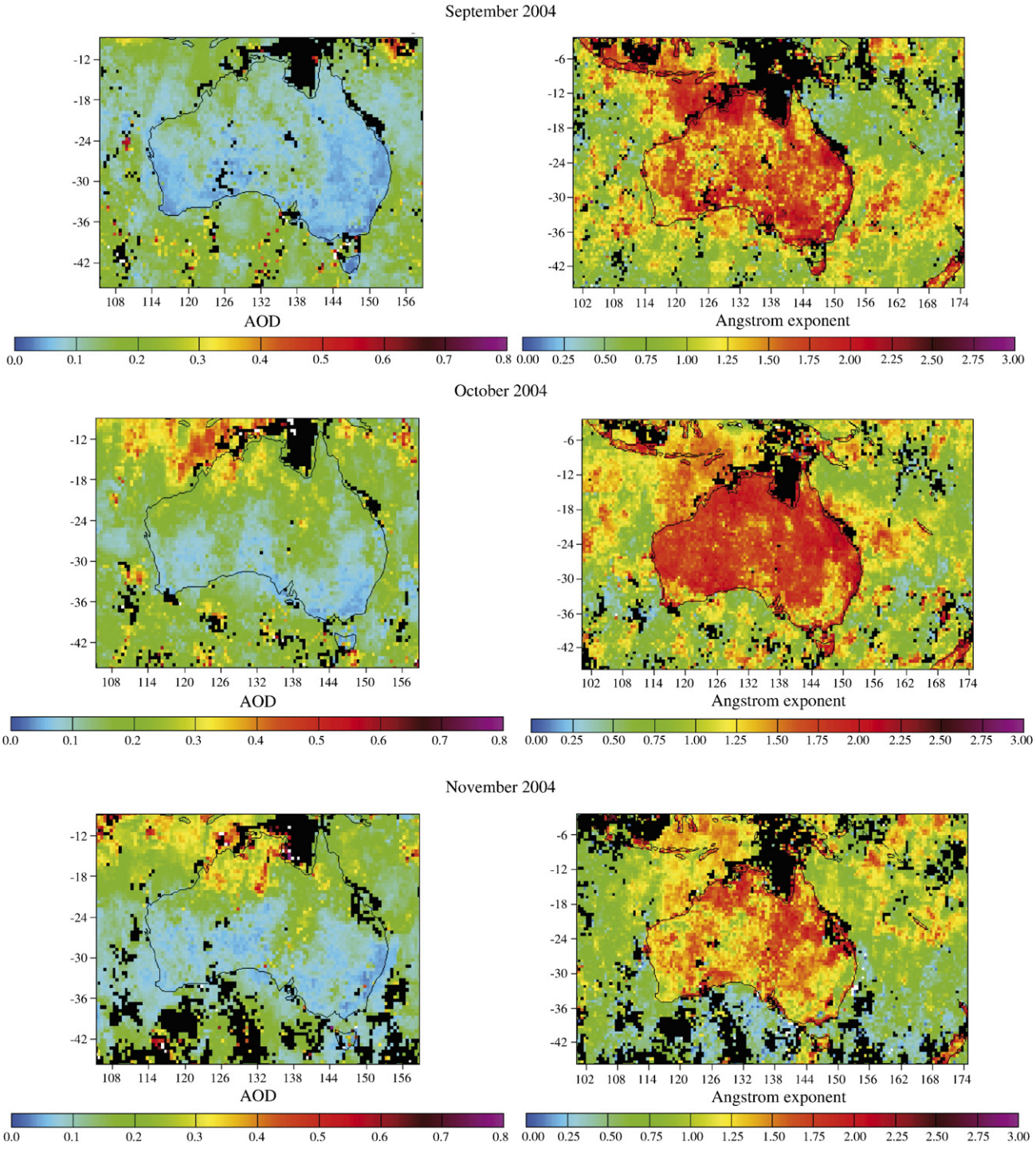

Fig. 3. MISR monthly averaged aerosol optical depth (green band AOD) – left column, and MISR monthly-averaged Angstrom parameter – right column, for Australian Spring 2004.

consists of a shaped polytetrafluoroethylene (PTFE) diffuser coupled to the entrance slit of the monochromator via a fibre optic bundle. The detector is a side-on photomultiplier tube operated in analogue mode and sampled by a 24 bit analogue-to-digital converter. The entire system is housed in a weather-proof thermally-insulated and electrically-shielded housing. The temperature of the system is held at 30±1 °C using thermoelectric coolers and resistive heaters. The spectro-radiometers are located at least 70 m from the nearest building or tree to ensure a near hemispherical field of view.

The spectroradiometers take scans at 5 degree intervals of solar zenith angle from 95° (morning twilight) to 95° (evening twilight) except during a 2 hour period around local noon when scans are taken every 15 min. The nominal spectral resolution is 0.65 nm. The scan range is from 285 nm to 450 nm in intervals of 0.2 nm. To reduce the effect of irradiance variation during a

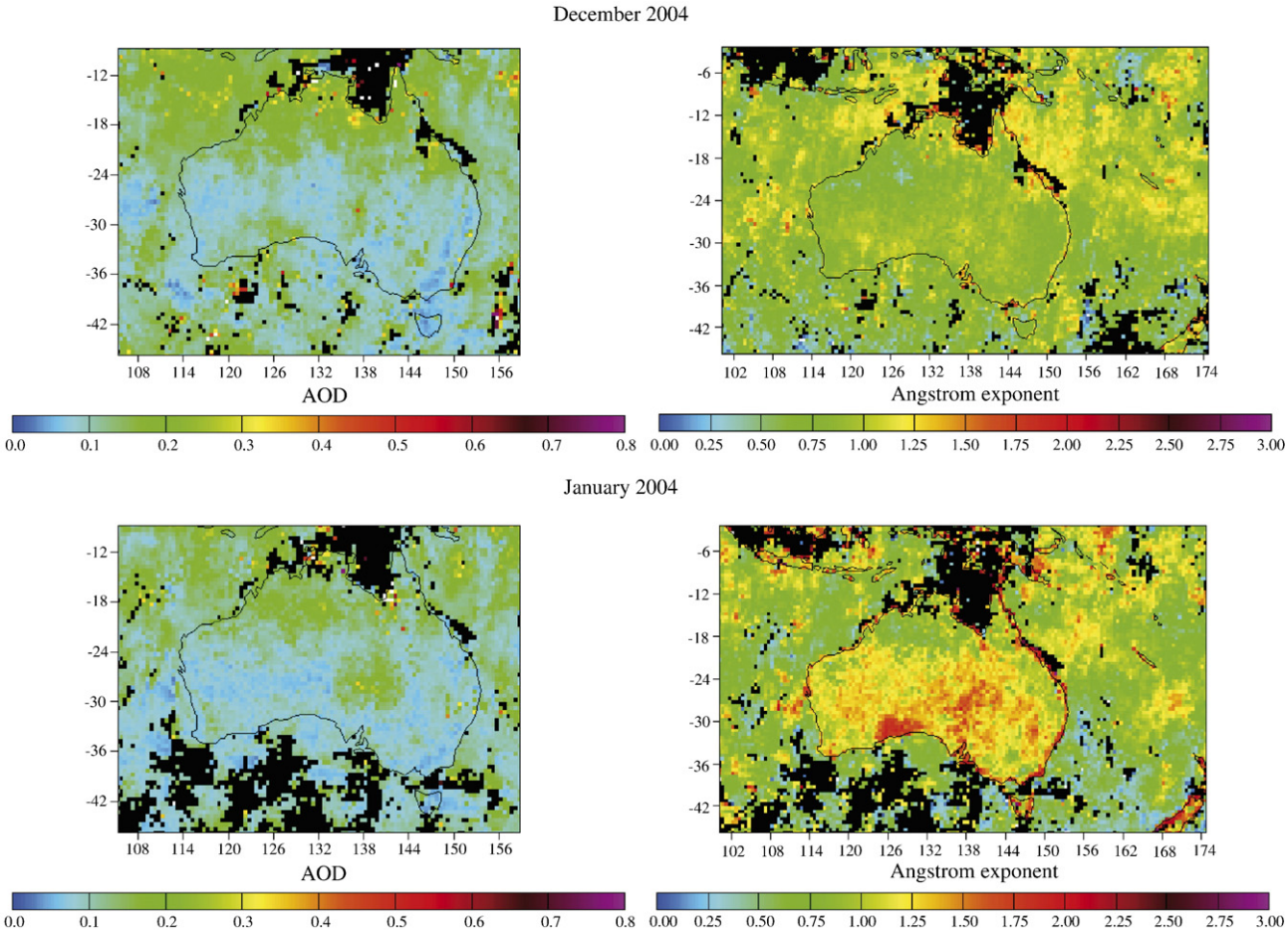

Fig. 4. MISR monthly-averaged aerosol optical depth (green band AOD) – left column, and MISR monthly-averaged Angstrom parameter – right column, for Australian Summer 2004.

scan, a reverse scan (450–285 nm) and a forward scan (285–450 nm) are averaged. The time taken for the reverse and forward scans is 272 s. The scan is time stamped at the center of the scan. Before and after the scan the monochromator is set to 150 nm (well below the solar cut-off) and 30 second averages are used to measure signal offsets.

The calibration of the instrument is checked weekly using a 45 W and a mercury lamp system (the calibration lamp unit, CLU). The irradiance calibration is adjusted when 3 successive weekly checks show a change of either 2% in the measured UV-B responsivity (apparent lamp irradiance) or 1% in the measured UV-A responsivity (apparent lamp irradiance). Every 6 months a suite of 4 transfer standard lamp units are used to check the performance of the CLU. The 4 transfer standard lamps have a NIST traceable calibration transferred to them by NIWA. Every year the CLU is replaced with one of the transfer lamp units and returned to NIWA for refurbishment and recalibration. The wavelength errors are reduced to be less than 0.05 nm using techniques described elsewhere (Liley & McKenzie, 1997).

4. Modeling approach and benchmark cases

Our approach compares surface UV irradiance spectra measured on days on which the overhead aerosol loading was significant at Darwin (smoke) and Alice Springs (dust and/or smoke) to surface UV irradiance spectra measured on days on which the aerosol loading at each site was as small as possible. Clear-sky model calculations for conditions (day of the year, SZA and overhead ozone column) corresponding to the measurements were used to remove differences in surface UV irradiances due to stratospheric ozone.

We simulated the clear-sky spectra using the libRadtran (Mayer & Kylling, 2005; Mayer et al., 2004) model, which allows for different input formats and varying the spectral resolution of the calculations for comparison with spectrally-resolved UV measurements. The model covers the wavelength range from 176 nm to 850 nm with resolution from 0.15 nm to 1 nm. The libRadtran package includes three different radiative transfer solvers. We used the general purpose discrete ordinate algorithm DISORT (8 streams) (Stamnes et al., 1988) for our calculations, assuming a vertically-inhomogeneous, non-isothermal, plane-parallel atmosphere. The most important parameters for modeling aerosol-free cloudless sky irradiances are the ozone column and surface albedo (molecular scattering was calculated for a fixed tropical atmosphere profile). Measured daily average ozone column values are available at both Darwin and Alice Springs, but an experimentally-determined surface albedo is not available for either site (and would be somewhat

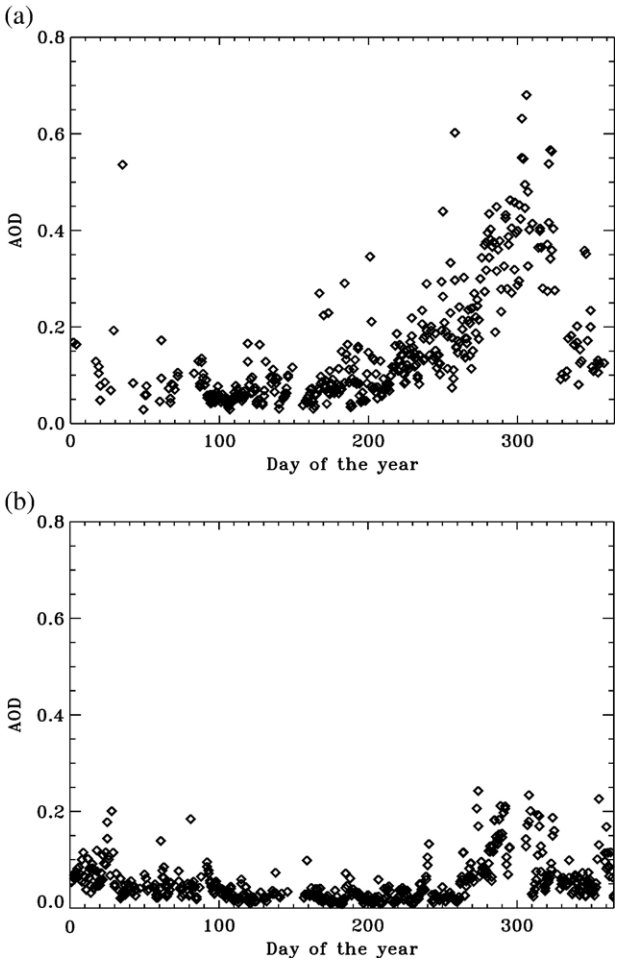

Fig. 5. Daily-averaged 500 nm AOD at (a) Darwin (b) Alice Springs as measured by BoM sunphotometers.

complicated to determine). For this study we used the spectrally-resolved albedo for grass that is included with libRadtran (Feister & Grewe, 1995). This albedo increases monotonically with increasing wavelength between 290 and 450 nm (0.016 at 290 nm, 0.018 at 350 nm, 0.022 at 400 nm, and 0.031 at 450 nm) (Feister & Grewe, 1995). The spectral dependence of this albedo and its magnitude are reasonably consistent (to within a factor of 2 for the magnitude and qualitatively for the spectral variation) with that deduced from comparisons between measured and modeled spectra of the diffuse to direct irradiance ratio at 300–450 nm for a New Zealand site which is covered with grass during summer (Zeng et al., 1994). The absolute albedo also is reasonably consistent with other ground-based and satellite-derived measurements (Krotkov et al., 1998) for sites with similar ground cover. For the extraterrestrial irradiance we used the standard libRadtran solar spectrum, which is the 0.15 nm resolution solar spectrum measured by the Solar Ultraviolet Spectral Irradiance Monitor (SUSIM) during the ATLAS 3 (<408 nm) and ATLAS 2 (>408 nm) missions in 1994 and 1993, respectively (Mayer & Kylling, 2005; VanHoosier, 1996). The tropical atmospheric profile was used for the simulations. We convolved the high resolution simulated spectra of the global irradiance with a triangular slit function whose FWHM was 0.6 nm to match the nominal spectrometer bandwidth. This markedly reduced the amplitude of high frequency structures in the ratio between measured and modeled spectra.

To test model vs. measurement discrepancies, we chose several days at the Darwin and Alice Spring sites when the optical depth derived from sunphotometer measurements was very low (less than 0.04 at 500 nm and less than 0.07 in the UV-A) and used these as benchmark cases for clear-sky conditions. Table 1 lists the selected days together with the measured AOD and overhead ozone column. After we introduced the instrument slit function into the model, we achieved good agreement between the model and measurements taken on all of the selected clear-sky days at Darwin. We found model/measurement differences to be less than 5% for all UV wavelengths (280–400 nm) of all spectra except near the calcium deep absorption lines at 393 and 397 nm. The agreement was not as good for the clear-sky cases at Alice Springs where UV-B model/measurement differences were as large as ~ 10%. Further study is required to identify probable causes for these differences. The two factors that are most likely to explain

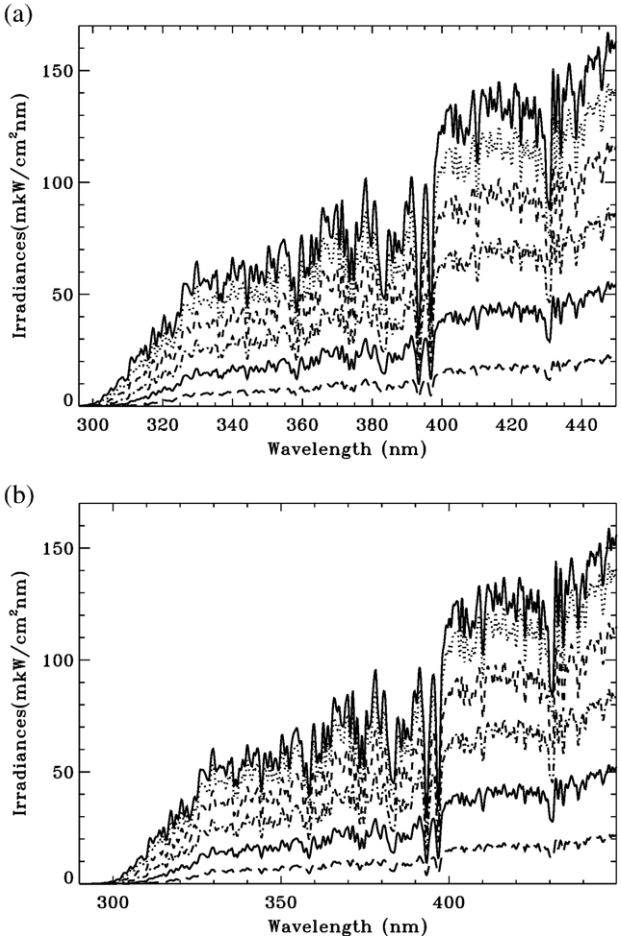

Fig. 6. Examples of BoM measured surface irradiance spectra: surface irradiances measured on (a) April 15, 2004, at Darwin site and (b) on April 11, 2004, at Alice Springs site. Irradiances shown at solar zenith angles (SZA)=30°, 40°, 50°, 60°, 70°, and 80° (largest irradiances correspond to the smallest SZA).

Table 1
Selected aerosol-free benchmark cases

Date in 2004	Location	Time of day	Selected SZAs (degrees)	AOD 500 nm	UV-A AOD 380 nm (Darwin) 367 (Alice Springs)	Ozone DU
April 15	Darwin	PM	22.3, 22.7, 23.6, 25.1	0.029–0.033	0.046–0.056	261.8
April 16	Darwin	AM	23.9, 25.4, 27.3, 29.5	0.028–0.035	0.043–0.053	261.5
April 17	Darwin	AM	23.3, 24.2, 27.5, 29.7	0.038–0.043	0.058–0.062	258.8
April 10	Alice Springs	AM	32.2, 34.2, 35.7, 40.0	0.032–0.033	0.041–0.044	247
April 11	Alice Springs	AM	32.2, 33.3, 36.0, 40.0	0.031–0.038	0.043–0.051	243
April 12	Alice Springs	AM	32.6, 33.7, 36.3, 40	0.035–0.040	0.049–0.054	245

the differences are uncertainties in the modeled vertical profile for the ozone column and the non-zero aerosol optical depth.

The latter of these is discussed further below. There are uncertainties in the modeled surface albedo but the actual surface reflectivity at UV wavelengths should be small, as discussed above, and even setting the model surface albedo to zero would decrease the modeled surface UV irradiances by less than 1.5% (Krotkov et al., 1998; Weihs & Webb, 1997), which is not sufficient to explain the observed UV-B difference of as much as 10%. The high-frequency, low-amplitude scatter of a few percent in the ratio spectra likely can be explained by either a small remaining difference between the model's and the instrument's bandwidths or a small offset in their wavelength scales. Examples of the measurement/model relations for two clear-sky cases that typify the model/measurement agreement at Darwin (a) and Alice Springs (b) are shown in Fig. 7. The remaining clear-sky cases we examined are listed in Table 1 and all look similar.

Krotkov et al. (1998) described the aerosol effect on global UV irradiances in terms of an aerosol attenuation factor (η), which they defined as:

$$F_{\text{aer}} = F_{\text{clear}}(1-\eta) \tag{1}$$

where F_{aer} and F_{clear} are surface UV global irradiances for aerosol-loaded and aerosol-free atmospheres, respectively. Rearranging to solve for η, Krotkov et al. (1998) also estimated a relationship between η and AI, the TOMS Aerosol Index:

$$\eta = 1-\frac{F_{\text{aer}}}{F_{\text{clear}}} = 1-\exp\left[-\frac{k}{b}\text{AI}\right] \tag{2}$$

with the latter half derived from the dependence of η and AI on aerosol optical depth, τ_a setting parameter $a=0$:

$$\eta = 1-\exp(-k\tau_a) \tag{3}$$

$$\text{AI} = a + b\tau_a \tag{4}$$

k and b are both functions of aerosol absorption but their ratio is a much weaker function of aerosol absorption. Based on calculations which assumed a single absorbing aerosol layer between 2 and 4 km altitude, Krotkov et al. (1998) found both dust and smoke had $k/b=0.2$–0.3 for SZA between 0 and 30°.

If we examine the components of F for a simplified situation, we can gain some insight into the sensitivity of the model calculations to various input parameters, as was demonstrated in numerical calculations (Krotkov et al., 1998), and see how the small aerosol optical depth present in our clear-sky benchmark

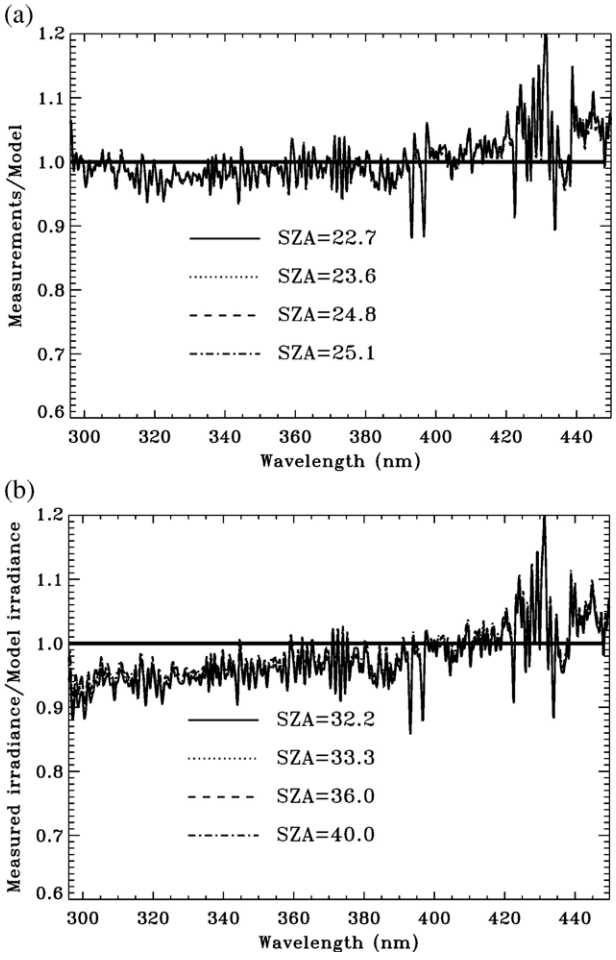

Fig. 7. Examples of comparisons between measured and modeled irradiances on clear-sky days (reported 500 nm AOD < 0.05): (a) April 15, 2004, Darwin, AOD at 500 nm = 0.030; (b) April 11, 2004, Alice Springs, AOD at 500 nm = 0.030. The quantity plotted is the measured global irradiance divided by the modeled clear-sky global irradiance. The modeled clear-sky global irradiance was calculated for the SZA and overhead ozone column corresponding to each measurement. No clouds or aerosols were included in the model calculations. The four ratios shown in (a) are for SZA = 22.7° (solid line), 23.6° (dotted line), 24.8° (dashed line), and 25.1° (dash-dot line). The four ratios shown in (b) are for SZA = 32.2° (solid line), 33.3° (dotted line), 36.0° (dashed line), and 40.0° (dash-dot line). The four ratios shown on each plot nearly agree and, thus, are almost indistinguishable.

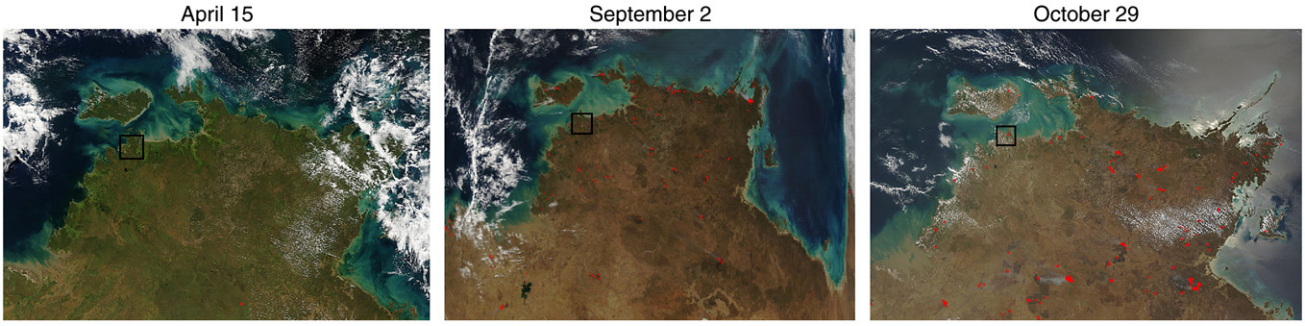

Fig. 8. MODIS fire detection examples: April 15, 2004 – clear sky, September 9, 2004 – downwind fires, October 29, 2004 – flaming fires at Darwin. Location of Darwin site is shown by a black open square. Red points mark the location of fires.

cases may lead to the observed differences from clear-sky model calculations.

$$F_{\text{surf}} = \frac{F_2}{(1-R_s S_b e^{-2\tau_b})} = F_1(1-S_c)e^{-\tau_c}\frac{1}{(1-R_s S_b e^{-2\tau_b})} \quad (5)$$

where F_{surf} is the downwelling surface UV irradiance, F_2 is the (downwelling) surface UV irradiance if the Earth's surface were completely absorbing, F_1 is the downwelling global UV irradiance entering the troposphere (i.e., entering the altitude layers where multiple scattering is important), R_s is the Earth's surface reflectivity (assuming it is Lambertian), S_b is the fraction of radiation reflected from the Earth's surface that is backscattered to the surface by the atmosphere, τ_b is one-half of the absorption optical depth along a photon's path from reflection at the Earth's surface through the atmosphere and back to the Earth's surface, S_c is the fraction of F_1 scattered back to space by the troposphere, τ_c is the absorption optical depth along a photon's path from the tropopause to the Earth's surface. The maximum of $S_b\exp(-2\tau_b)$ in the Near UV for a clear sky is about 0.4 and occurs at around 320 nm (Krotkov et al., 1998). Taking a ratio of surface UV irradiances from an aerosol-loaded case and a clear-sky case and assuming all other atmospheric conditions remain the same gives:

$$\frac{F_{\text{aer}}}{F_{\text{clear}}} = \frac{(1-S_c(\text{aer}))e^{-\tau_c(\text{aer})}}{(1-S_c(\text{clear}))e^{-\tau_c(\text{clear})}}\frac{(1-R_s(\text{clear})S_b(\text{clear})e^{-2\tau_b(\text{clear})})}{(1-R_s(\text{aer})S_b(\text{aer})e^{-2\tau_b(\text{aer})})} \quad (6)$$

If $R_s = 0.05$ (Herman et al., 2001; Zeng et al., 1994), the second term on the right hand side will be in the range of 0.98–1.03. For smaller R_s (Feister & Grewe, 1995; Herman et al., 2001) or small aerosol optical depths (S_b (aer) $\approx S_b$(clear) and τ_b (aer) $\approx \tau_b$ (clear)), the range is much smaller and this term can be set to unity. The strong forward scattering exhibited by most non-absorbing aerosols suggests that the addition of a small optical depth of non-absorbing aerosols to a clear-sky atmosphere will not cause S_c (aer) to differ significantly from S_c(clear), which is what is found in numerical calculations where a large majority of the extinction of the direct beam due to non-absorbing aerosol scattering is compensated by a corresponding increase in the diffuse irradiance at the surface (Krotkov et al., 1998). Addition of a small optical depth of absorbing aerosols, however, should decrease $F_{\text{aer}}/F_{\text{clear}}$ by an amount that is approximately linearly proportional to the absorption optical depth. Thus, an absorbing aerosol with UV-A extinction optical depth of about 0.05 may produce a significant decrease in $F_{\text{aer}}/F_{\text{clear}}$ at UV-B wavelengths if a majority of the extinction is due to absorption. This might explain a large fraction of the measurement/model difference in Fig. 7b, but we would need more detailed information than we have available to explain why we have good agreement for the clear-sky cases at Darwin but not at Alice Springs.

The discussion in Section 7 uses clear-sky model calculations as a surrogate for F_{clear} in Eq. (2) and computes η for selected cases so our results may be compared to the results from Krotkov et al. (1998). Sections 5 and 6 report our results in

Table 2
Selected downwind low aerosol-loading cases at Darwin

Date in 2004	Time of day	Selected SZAs (degrees)	AOD 500 nm	Angstrom parameter	AOD 380 nm	Ozone DU
August 28	PM	27.0, 29.3, 35.0	0.18–0.20	1.16–1.17	0.34–0.39	251.8
August 30	AM	25.7, 28.0, 30.0, 35.0	0.17–0.20	1.24–1.26	0.34–0.39	241.7
September 1	AM	25.2, 27.5, 30, 35	0.21–0.22	1.45–1.47	0.41–0.42	245.3
September 2	PM	23.0, 25.0, 30.0, 35	0.15–0.16	1.47–1.5	0.28–0.33	250.2
September 9	AM	23.9, 30, 35, 40	0.15–0.18	1.73–1.76	0.29–0.36	256.0

Table 3
Selected flaming fires high aerosol-loading cases at Darwin

Date in 2004	Time of day	Selected SZAs (degrees)	AOD 500 nm	Angstrom parameter	AOD 380 nm	Ozone DU
September 6	AM	23.9, 26.4, 30, 35	0.42–0.45	1.91–1.93	0.76–0.78	273.0
October 28	PM	21.9, 25, 30, 35, 40	0.43–0.44	1.41–1.45	0.57–0.60	262.7
October 29	AM	25, 30, 35, 40	0.59–0.65	1.38–1.41	0.81–0.86	271.0
October 30	AM	35, 40	0.62–0.63	1.53–1.58	0.86–0.88	269.7
November 2	AM	25, 30, 35, 40	0.56–0.59	1.39–1.42	0.87–0.89	267.0
November 14	PM	25, 30, 35, 40	0.39–0.41	1.48–1.53	0.57–0.59	257.5
November 17	AM	25, 30, 35, 40	0.45–0.47	1.65–1.68	0.70–0.73	257.7

terms of a ratio between measured surface UV irradiances on days with significant aerosol loading and days with minimal aerosol loading with model calculations used as a surrogate for F_{clear}.

$$\frac{F_{a1}/F_{c1}}{F_{a2}/F_{c2}} = \frac{(1-S_c(a1))e^{-\tau_c(a1)}}{(1-S_c(c1))e^{-\tau_c(c1)}} \frac{(1-S_c(c2))e^{-\tau_c(c2)}}{(1-S_c(a2))e^{-\tau_c(a2)}} \quad (7)$$

$$\frac{(1-R_s(c1)S_b(c1)e^{-2\tau_b(c1)})}{(1-R_s(a1)S_b(a1)e^{-2\tau_b(a1)})} \frac{(1-R_s(a2)S_b(a2)e^{-2\tau_b(a2)})}{(1-R_s(c2)S_b(c2)e^{-2\tau_b(c2)})}$$

where a1 is the significant aerosol loading measurement, a2 is the minimal aerosol loading measurement, c1 is the clear-sky case corresponding to a1, and c2 is the clear-sky case corresponding to a2. If the tropospheric ozone column and distribution are not greatly different for c1 and c2, then the ratio of clear-sky terms involving the surface albedo will be approximately unity with a high degree of accuracy due to the low surface albedo. The maximum difference in measured ozone column abundance between our clear-sky benchmark cases and our significant aerosol-loading cases is about 20 Dobson Units (DU). If 15% of this column total change occurs in the troposphere, then sensitivity calculations (Krotkov et al., 1998) suggest the ratio $\exp(-\tau_c(c2))/\exp(-\tau_c(c1))$ will be within the range 0.98–1.02 at 290 nm and closer to unity at longer wavelengths. The measured surface pressures at Darwin and Alice Springs differed from the nominal values in the tropical model for 30 m and 546 m elevation, respectively, by less than 10 mb on the days selected. These deviations from the nominal pressure altitudes should produce deviations from the modeled Rayleigh scattering which result in less than a 1.5% change in surface irradiance at 290–330 nm (Krotkov et al., 1998). Based on the conditions applicable to our measurements,

$$\frac{F_{a1}/F_{c1}}{F_{a2}/F_{c2}} \approx \frac{(1-S_c(a1))e^{-\tau_c(a1)}}{(1-S_c(a2))e^{-\tau_c(a2)}} \frac{(1-R_s(a2)S_b(a2)e^{-2\tau_b(a2)})}{(1-R_s(a2)S_b(a1)e^{-2\tau_b(a1)})} \quad (8)$$

If the minimal aerosol loading case, a2, is sufficiently close to a clear-sky situation, then Eq. (8) becomes $\approx F_{a1}/F_{\text{clear}}$. The impact of uncertainties in measuring input parameters for the model calculations, such as overhead ozone column, has not been considered above but are examined in numerical calculations presented in Krotkov et al. (1998).

5. UV effects of smoke particles at Darwin

The initial part of this investigation concentrated on the effects of smoke for selected days at the Darwin site. We selected three types of cases for model measurement comparisons: clear-sky, low aerosol loading, and high aerosol loading using MODIS fire maps and sunphotometer AOD daily-averaged values for the period January–December of 2004.

Terra MODIS and Aqua MODIS (Salomonson et al., 2002) observe the Earth in 36 spectral bands from 0.4 to 14.4 μm. Terra's orbit around the Earth is timed so that it passes from north to south across the equator in the morning, while Aqua passes south to north over the equator in the afternoon. Terra MODIS and Aqua MODIS scan pattern sees a 2330 km swath, providing global coverage of the Earth's surface every 1 to 2 days. MODIS fire detection products (Justice et al., 2002), which are based on 4 to 11 μm brightness temperatures, were used in our study. Fig. 8 shows examples of a MODIS fire detection over Darwin for clear sky (April 15, 2004, no hot

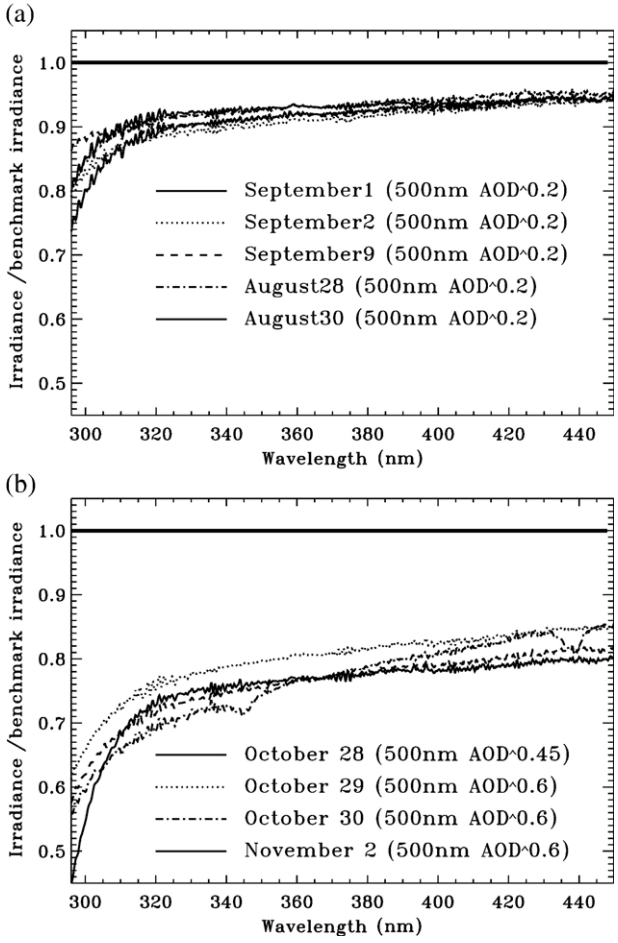

Fig. 9. Examples for Darwin of ratios between (a) irradiances on days with low aerosol loadings (sunphotometer AOD at 500 nm ~ 0.15–0.20) and clear-sky benchmark irradiances for SZA=25° and (b) irradiances on days with high aerosol loadings (sunphotometer AOD at 500 nm ~ 0.55–0.60) and clear-sky benchmark irradiances for SZA=25°. The numerator of the quantity plotted is the measured global irradiance divided by the modeled clear-sky global irradiance. The denominator of the quantity plotted is the measured clear-sky benchmark global irradiance divided by the modeled clear-sky benchmark global irradiance. All measured irradiances were measured at the Darwin site. The clear-sky benchmark irradiances were measured on April 15, 2004, with AOD at 500 nm=0.030. The modeled clear-sky global irradiances were calculated for the SZA and overhead ozone column corresponding to each measurement. No clouds or aerosols were included in the model calculations. The measured irradiances are divided by modeled irradiances to remove the effects of differences in ozone column as described in the text prior to computing the ratios shown in the figure. The irradiances in (a) were measured in 2004 on August 28 (dotted line, AOD at 500 nm=0.22), August 30 (dashed line, AOD at 500 nm=0.19), September 1 (solid line, AOD at 500 nm=0.21), September 2 (dotted line, AOD at 500 nm=0.13), and September 9 (dashed line, AOD at 500 nm=0.18). The irradiances in (b) were measured in 2004 on October 28 (solid line, AOD at 500 nm=0.59), October 29 (dotted line, AOD at 500 nm=0.64), October 30 (dashed line, AOD at 500 nm=0.61), and November 2 (dotted line, AOD at 500 nm=0.61).

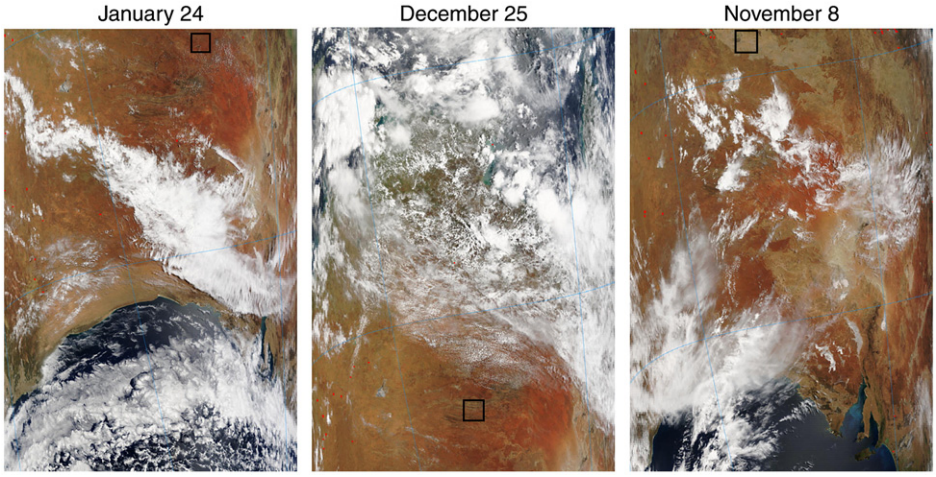

Fig. 10. MODIS fire detection around Alice Springs. Location of Alice Springs is shown by a black open square.

points), downwind fires (September 2, 2004) and flaming fires next to Darwin (October 29, 2004). The red marks on Fig. 8 indicate locations of active fires.

We examined all measured points of the Darwin sunphotometer AOD time series for each selected day and chose solar zenith angles (SZAs) where the AOD had minimum variability to use for our study. We chose SZAs where the optical depth was nearly constant for several hours. We restricted ourselves to UV spectra measured at SZAs less than 40° because the uncertainties in both the measured and the modeled spectra are smallest for SZAs close to local noon.

To study the differences between the spectral signature of smoke downwind and in close proximity to active bush fires, we chose two sets of smoky days from the MODIS Rapid Response System fire maps:

- Low aerosol loading — downwind fires
- High aerosol loadings — flaming fires near the site.

Tables 2 and 3 summarize the selected days for each set, together with reported AODs and Angstrom parameters at the selected SZAs and the measured overhead daily average ozone column values, which were used in the libRadtran model.

We compared cases of measured downwind smoke irradiances (examples are August 28, August 30, September 1, 2, 9, AOD ~ 0.15–0.2) and cases of measured flaming fires irradiances (examples are October 28, October 29, October 30, November 2, AOD ~ 0.6) to benchmark clear-sky irradiance spectra (AOD ~ 0, 03) measured on April 15 after ratioing each measured spectrum by the appropriate modeled clear-sky spectrum to remove ozone effects.

Fig. 9 demonstrates our general findings. The overall spectral signature seems to be very similar for the near source and downwind fires. The total effect increases with decrease of wavelength so UV-B attenuation in all analyzed cases is about 10% larger than the UV-A attenuation for downwind (AOD ~ 0.2)

Table 4
Selected aerosol-loading cases at Alice Springs

Date in 2004	Time of day	Selected SZAs (degrees)	AOD 500 nm	Angstrom parameter	AOD 380 nm	Ozone DU
January 24	PM	25, 30, 35, 40	0.11–0.12	0.06–0.08	0.12–0.13	262.7
November 9	PM	25, 30, 35, 40	0.16–0.18	1.15–1.20	0.22–0.24	265.3
December 25	AM	25, 30, 35, 40	0.11–0.17	0.25–0.30	0.13–0.19	257.7

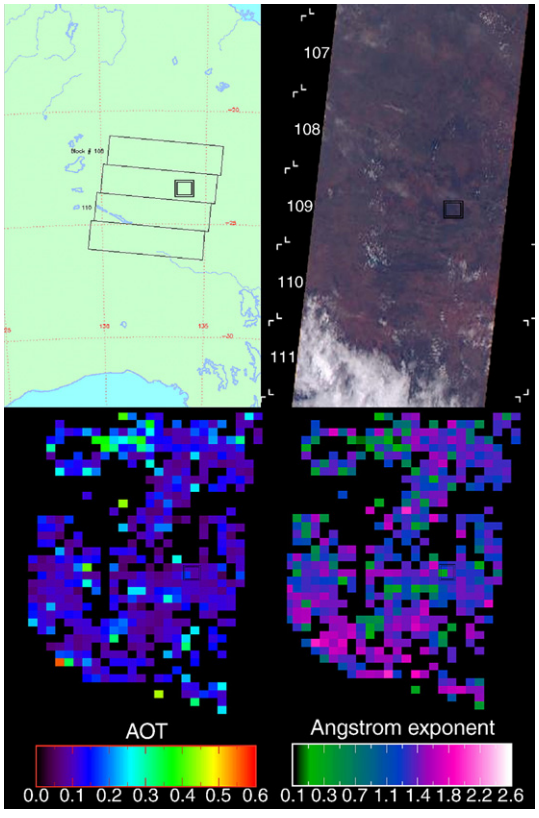

Fig. 11. MISR overpass on January 24, 2004. Path 103, orbit 21810, blocks 108–111. MISR RGB, green-band AOD and Angstrom parameter. Location of Alice Spring site is shown by a black open square.

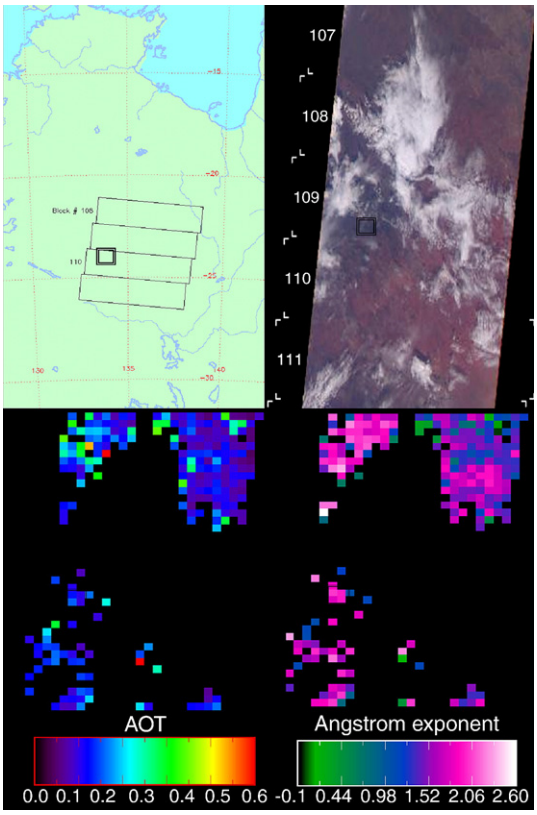

Fig. 12. MISR overpass on November 9, 2004. Path 101, orbit 26003, blocks 108–111. MISR RGB, green-band AOD and Angstrom parameter. Location of Alice Spring site is shown by a black open square.

cases and about 20% larger for flaming fires (AOD ~ 0.6) cases. We found that for otherwise similar atmospheric conditions, smoke aerosols at Darwin reduced the UV irradiance by 40−50% in the UV-B and 20–25% in the UV-A near active fires (AOD ~ 0.6), and by 15–25% in the UV-B and ~ 10% in the UV-A downwind of fires (AOD ~ 0.2). Some of the differences between spectra at the same AOD may reflect differences in particle properties, based on the differences in Angstrom parameter derived from the sunphotometer data. Other differences between spectra at the same AOD may be due to small variations in the AOD over the duration of the 4.5 minute instrument scan (e.g., the possible movement of a small cloud or small variations in aerosol loadings). The total smoke effect increases with an increase in the optical depth as expected; surface UV-A irradiance decreases in the presence of smoke aerosols from about 10% for AOD of 0.2 (Fig. 9(a)) to 20% for AOD of 0.45 (not shown) and up to 30% for AOD of 0.6 (Fig. 9(b)).

6. UV effects of different aerosol types at Alice Springs

Selection of dusty cases at Alice Springs was difficult because the total aerosol loadings were relatively low at this site throughout 2004 as shown in Fig. 5(b). We chose several days with moderate to high values of optical depth (AOD ~ 0.15) and then examined the aerosol properties using MODIS fire maps, the Angstrom parameter derived from sunphotometer measurements, and MISR aerosol retrievals.

From the sunphotometer measurements we determined that periods with moderate to high values for optical depth occurred on January 24–26, November 8–10, and December 24–26 in 2004. From these periods we selected days when MISR had coverage over Alice Springs so MISR data could provide contextual information (such as the locations of aerosol plumes) and information on aerosol properties. MISR had overpasses on January 24 (path 103, orbit 21810), November 9 (path 102, orbit 26003), and December 25 (path 103, orbit 26703). We selected these three days as our aerosol-loaded cases and compared the UV irradiances measured on those days to the benchmark clear-sky case at Alice Springs (April 11, 2004, AOD ~ 0.03).

Next, we examined MODIS fire maps to determine the locations of fires near Alice Springs. MODIS maps (see Fig. 10) indicate there were no fires on January 24 near Alice Springs but there were fires around Alice Springs on November 9 and Alice Springs may have been downwind of fires on December 25. The presence of downwind smoke at Alice Springs on December 25 (also a period of dust activity) is less certain and depends on the wind direction. The aerosol properties derived from sunphotometer measurements on these three days together with the ozone column values measured by TOMS are summarized in Table 4. The Angstrom parameter was low on January 24 and December 25 and high on November 9 confirming that November 9 was a smoky day. The aerosol AOD was only moderate, ~ 0.13, on January 24 and December 25, which makes aerosol property analysis difficult.

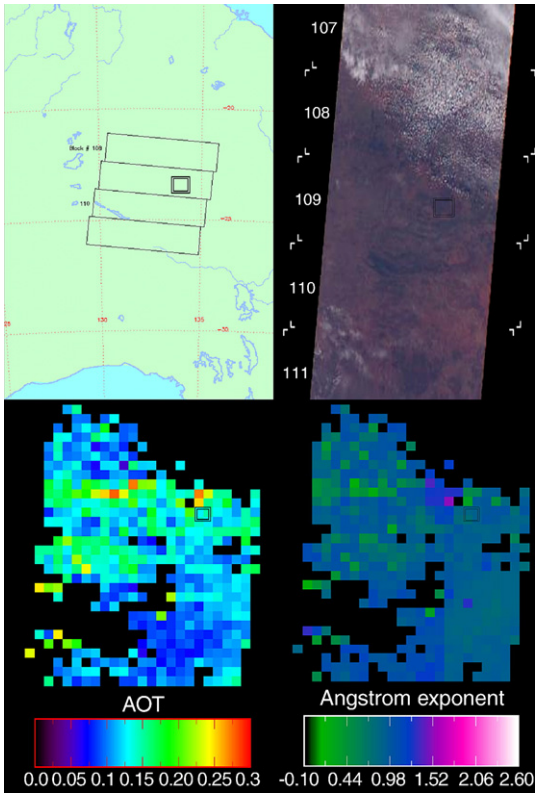

Fig. 13. MISR overpass on December 25, 2004. Path 103, orbit 26703, blocks 108–111. MISR RGB, green-band AOD and Angstrom parameter. Location of Alice Spring site is shown by a black open square.

The locations of MISR overpasses and the AOD and Angstrom parameter retrieved from the MISR data are shown on Figs. 11–13 for January 24, November 9, and December 25, respectively. MISR retrievals on January 24 show a moderate value for optical depth and low Angstrom parameter north of Alice Springs, which probably indicates there is dust over Alice Springs. On November 9 the MISR retrievals indicate a moderate value for AOD (~ 0.2) and high Angstrom parameter near Alice Springs in agreement with MODIS fire maps and the sunphotometer data. On December 25 MISR found a plume of aerosol northwest of Alice Springs with both a moderate value for optical depth and low Angstrom parameter in the plume. The Angstrom parameter is low over Alice Springs indicating the possible presence of dust particles there also. However, both the January 24 and December 25 retrievals may be affected by cirrus that was not detected by the cloud screening algorithm.

The AODs on all three days (January 24, November 9, and December 25) are similar but the reduction of the surface irradiance on November 9 is almost 15% stronger than on January 24 and December 25 (Fig. 14). This suggests smoke attenuates UV radiation more strongly than dust. However, more cases (preferably with higher aerosol loadings) are needed to fully assess the differences between dust and smoke for their effect on UV irradiances at Alice Springs.

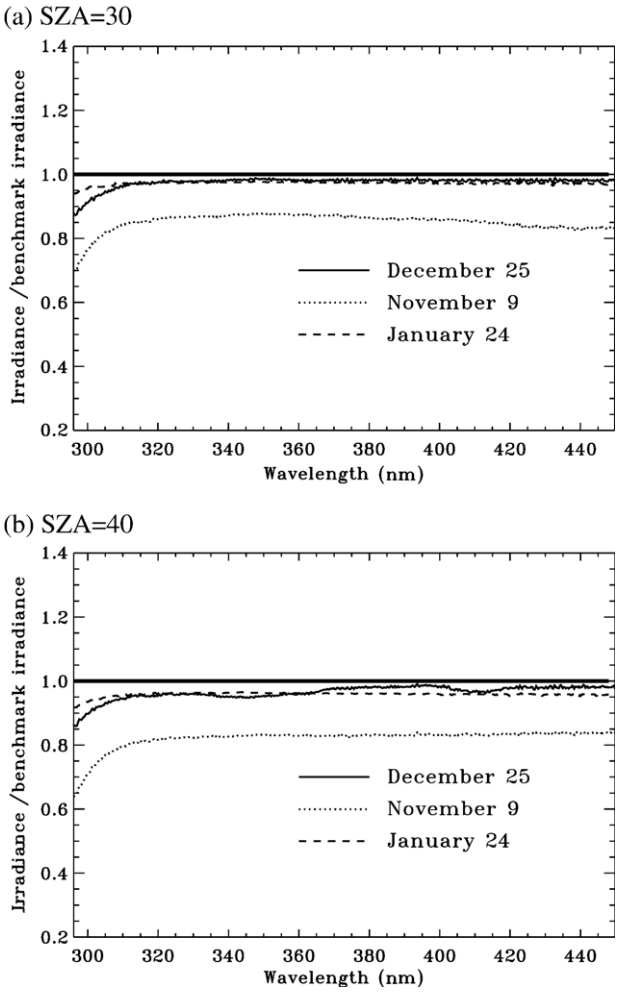

Fig. 14. Examples for Alice Springs of ratios between irradiances on days with moderate aerosol loadings and clear-sky benchmark irradiances: (a) SZA = 30° and (b) SZA = 40°. The numerator of the quantity plotted is the measured global irradiance divided by the modeled clear-sky global irradiance. The denominator of the quantity plotted is the measured clear-sky benchmark global irradiance divided by the modeled clear-sky benchmark global irradiance. All measured irradiances were measured at the Alice Springs site. The clear-sky benchmark irradiances were measured on April 11, 2004, with AOD at 500 nm = 0.030. The modeled clear-sky global irradiances were calculated for the SZA and overhead ozone column corresponding to each measurement. No clouds or aerosols were included in the model calculations. The irradiances were measured in 2004 on January 24 (dashed line, AOD at 500 nm = 0.11, mineral dust), November 9 (dotted line, AOD at 500 nm = 0.18, smoke), and December 25 (solid line, AOD at 500 nm = 0.13, mineral dust). The measured irradiances are divided by modeled irradiances to remove the effects of differences in ozone column as described in the text prior to computing the ratios shown in the figure.

7. Discussion and summary

From our analysis of the effect of smoke on surface UV irradiance at Darwin for a range of aerosol loadings, we found that the effect of smoke depends on wavelength and is strongest in the UV-B. Smoke aerosols have similar spectral signatures for flaming and downwind fires and its effect increases with increasing optical depth. Strong fires (AOD at 500 nm ~ 0.6) reduced irradiances by as much as 30% in the UV-A and by as much as 45% in the UV-B. The similarity of spectral signatures for flaming and downwind fires near Darwin is qualitatively consistent with the moderate rate of hygroscopic growth in scattering measured for smoke from a savanna woodland fire in Australia's Northern Territory in October 1997 (Gras et al., 1999).

Our analysis of surface irradiances at Alice Springs is not as conclusive. The cases we examined suggest a stronger reduction of surface irradiance by smoky aerosol mixtures compared to dusty aerosol mixtures. However, cases with higher dust loading are needed to make more reliable assessments of the aerosol type and properties and of their effects on surface UV irradiance.

Our comparison of the effect of aerosols on surface UV between Darwin and Alice Springs for the same visible AOD (November 9 at Darwin vs. September 9 at Alice Springs, AOD at 500 nm ~ 0.18) and (September 2 at Darwin vs. January 24 and December 25 at Alice Springs AOD at 500 nm ~ 0.13) show 10 to 20% differences in surface irradiances as shown in Fig. 15. That partially might be explained by differences in UV absorption of dust vs. smoke (smoke AOD could be as much as three times larger at 300 nm vs. 500 nm while the dust AOD is only about 20% larger at 300 nm vs. 500 nm). However, differences in atmospheric profiles or other factors at these two sites might account for at least part of these differences. Our findings suggest that even in cases of low aerosol loading, aerosol type (air mass characteristics) influences the spectral distribution of UV radiation and should be considered when modeling photochemical processes and biological exposure in Australia.

Using model calculations as a surrogate for clear-sky irradiances in Eq. (2), we have calculated the aerosol attenuation factor, η, for several cases, Fig. 16(a) shows results for smoke and (b) shows results for dust. The dust aerosol attenuation factors at 340–380 nm for the 2 days shown in (b) are ~ 0.05–0.10, which

is below the minimum threshold of 0.20 that Krotkov et al. (1998) used to identify significant reductions in surface UV due to aerosol absorption. The dust aerosol attenuation factors on our 2 days were also much smaller than those calculated based on Saharan dust (Krotkov et al., 1998). The smoke aerosol attenuation factors at 340–380 nm for the days shown in (a) are larger than those for our two dust cases. The largest values at 340–380 nm, ~ 0.25–0.30, are roughly comparable to those found for aerosols over Sub-Saharan Africa but smaller than those found over the Amazon (Krotkov et al., 1998). The large aerosol attenuation factor for smoke over Darwin and the frequent occurrence of days with AOD at 500 nm greater than 0.4 suggests smoke aerosols are important for understanding surface UV irradiances in northern Australia. Previous research had found that

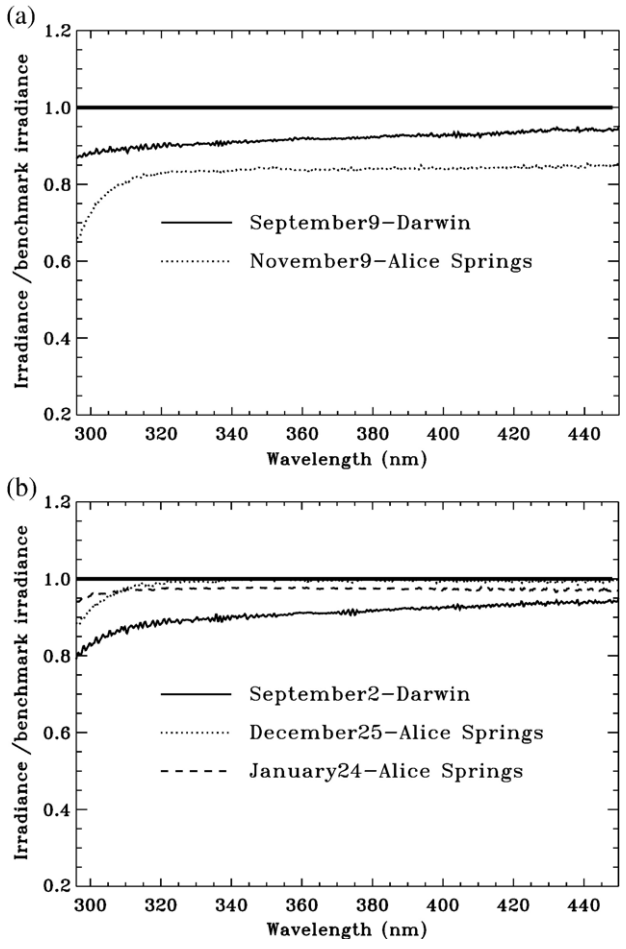

Fig. 15. Comparisons of UV attenuation at Alice Springs and Darwin (SZA=35°). Ratios between irradiances on days with moderate aerosol loadings and clear-sky benchmark irradiances: (a) September 9, 2004 (solid line, Darwin, AOD at 500 nm=0.18, smoke, Angstrom parameter=1.73–1.76) and November 9, 2004 (dotted line, Alice Springs, AOD at 500 nm=0.18, smoke, Angstrom parameter=1.15–1.20) and (b) January 24, 2004 (dashed line, Alice Springs, AOD at 500 nm=0.11, mineral dust), September 2, 2004 (solid line, Darwin, AOD at 500 nm=0.13, smoke), and December 25, 2004 (dotted line, Alice Springs, AOD at 500 nm=0.13, mineral dust). The numerator of the quantity plotted is the measured global irradiance divided by the modeled clear-sky global irradiance. The denominator of the quantity plotted is the measured clear-sky benchmark global irradiance divided by the modeled clear-sky benchmark global irradiance.

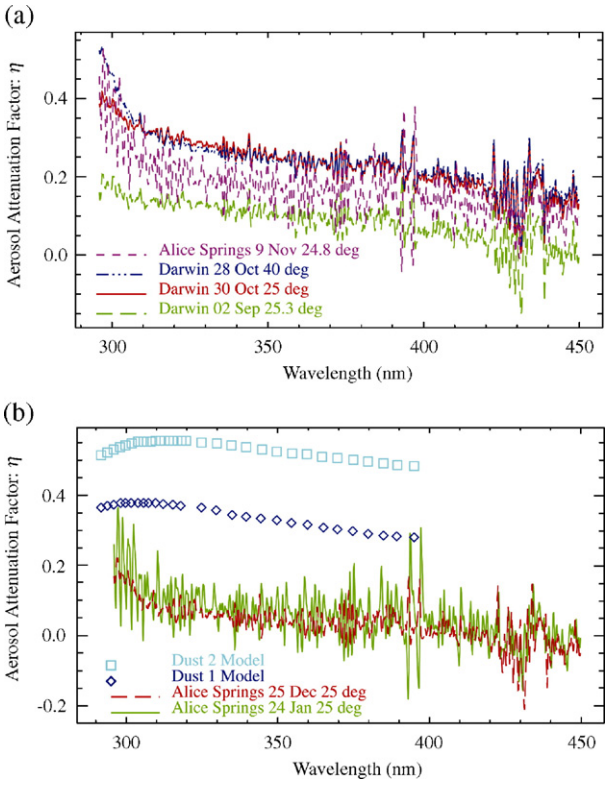

Fig. 16. Aerosol attenuation factor, η, for selected measurements. The aerosol attenuation factor is defined by Eq. (2) with model calculated irradiance used for the clear-sky term. (a) Smoke cases. September 2, 2004 (long dashed line, Darwin, AOD at 500 nm=0.15–0.16, SZA 25.3°), October 28, 2004 (dash triple dot line, Darwin, AOD at 500 nm=0.43–0.44, SZA 40°), October 30, 2004 (solid line, Darwin, AOD at 500 nm=0.62–0.63, SZA 25°), and November 9, 2004 (short dashed line, Alice Springs, AOD at 500 nm=0.16–0.18, SZA 24.8°) and (b) dust cases. January 24, 2004 (solid line, Alice Spring, AOD at 500 nm=0.11–0.12, SZA 25°) and December 25, 2004 (long dashed line, Alice Springs, AOD at 500 nm=0.11–0.17, SZA 25°). Dust 1 and Dust 2 are model calculations based on Saharan dust (Krotkov et al., 1998).

carbonaceous aerosols over northern Australia may be important for understanding the regional (and maybe global) climate (O'Brien & Mitchell, 2003).

Our current analysis was based on total (diffuse plus direct) irradiances measured by BoM spectroradiometers. In latter half of 2006, the BoM plans to start measuring diffuse and direct irradiances separately. These measurements should permit retrieval of more detailed UV aerosol properties using, for example, an optimal estimation technique (Goering et al., 2005), which is based on the TUV4.2 radiative transfer model. Retrieval of UV aerosol properties, such as single-scattering albedo, would enhance our analysis and provide additional constraints for assessing the effects of aerosols on surface UV irradiances.

Acknowledgments

We thank Dr. Ross Mitchell for his efforts in establishing and maintaining the CSIRO AGSNet sunphotometer site at Darwin, and we thank Dr. Bruce Forgan for his efforts in establishing and maintaining the BoM sunphotometers at Darwin and Alice Springs. We also thank Dr. Forgan for a critical reading of the

manuscript. This research was supported partially by a grant from the NASA New Investigator Program in Earth Science under M.-Y. Wei. Part of this work was performed at the Jet Propulsion Laboratory, California Institute of Technology, under contract to the National Aeronautics and Space Administration. Grants to FPM from The Ian Potter Foundation, the International Society of Biometeorology, and the Australian Research Council partially supported travel to develop this research project. The MISR data were obtained from the NASA Langley Research Center Atmospheric Sciences Data Center.

References

Balis, D., Amiridis, V., Zerefos, C., Kazantzidis, A., Kazadzis, S., Bais, A., et al. (2004). Study of the effect of different type of aerosols on UV-B radiation from measurements during EARLINET. *Atmospheric Chemistry and Physics*, *4*, 302−321.

BoM (2003). Bushfire weather. Australian Bureau of Meteorology publications. http://www.bom.gov.au/lam/weathed.shtml

Craig, R., Heath, B., Raisbeck-Brown, N., Steber, M., Marsden, J., Smith, R., 2002. *The distribution, extent and seasonality of large fires in Australia, April 1998–March 2000, as mapped from NOAA-AVHRR imagery.* Australia State of the Environment Second Technical Paper Series (Bio diversity), Department of the Environment and Heritage Australian fire regimes: contemporary patterns (April 1998– March 2000) and changes since European settlement, http://www.ea.gov.au/soe/techpapers/index.html

Diaz, J. P., Exposito, F. J., Torres, C. J., Carrena, V., & Redondas, A. (2000). Simulations of the mineral dust effect on the UV radiation level. *Journal of Geophysical Research*, *105*, 4979−4991.

Dickerson, R., Kondragunta, S., Stenchikov, G., Civerolo, K., Doddridge, B., & Holben, B. (1997). The impact of aerosols on solar ultraviolet radiation and photochemical smog. *Science*, *278*, 827−830.

Diner, D. J., Asner, G., Davies, R., Knyazikhin, Y., Muller, J., Nolin, A., et al. (1999). New directions in Earth observing: Scientific applications of multiangle remote sensing. *Journal of Geophysical Research*, *80*, 2209−2228.

Diner, D. J., Beckert, J., Reilly, T., Bruegge, C., Conel, J., Kahn, R., et al. (1998). Multi-angle Imaging SpectroRadiometer (MISR) instrument description and experiment overview. *IEEE Transactions on Geoscience and Remote Sensing*, *36*, 1072−1087.

Feister, U., & Grewe, R. (1995). Spectral albedo measurements in the UV and visible region over different types of surfaces. *Photochemistry and Photobiology*, *62*, 736−744.

Gies, P., Roy, C., Javorniczky, J., Handerson, S., Lemus-Deschamps, L., & Driscoll, C. (2004). Global solar UV index: Australian measurements, forecasts and comparison with the UK. *Photochemistry and Photobiology*, *79*, 32−39.

Goering, C. D., L'Ecuyer, T., Graeme, L. S., Slusser, J. R., Scott, G., Davis, J., et al. (2005). Simultaneous retrievals of column ozone and aerosol optical properties from direct and diffuse solar irradiance measurements. *Journal of Geophysical Research*, *110*, D05204.

Gras, J. L., Jensen, J. B., Okada, K., Ikegami, M., Zaizen, Y., & Makino, Y. (1999). Some optical properties of smoke aerosol in Indonesia and tropical Australia. *Geophysical Research Letters*, *26*, 1393−1396.

Herman, J. R., Bhartia, P. K., Torres, O., Hsu, C., Seftor, C., & Celarier, E. (1997). Global distribution of UV-absorbing aerosols from nimbus-7/TOMS data. *Journal of Geophysical Research*, *102*, 16911−16922.

Herman, J. R., Celarier, E., & Larko, D. (2001). UV 380 nm reflectivity of the earth's surface, clouds and aerosols. *Journal of Geophysical Research*, *106*, 5335−5351.

Justice, C. O., Giglio, L., Korontzi, S., Owens, J., Morisette, J. T., Roy, D., et al. (2002). The MODIS fire products. *Remote Sensing of Environment*, *83*, 244−262.

Kahn, R., Banerjee, P., & McDonald, D. (2001). The sensitivity of multiangle imaging to natural mixtures of aerosols over ocean. *Journal of Geophysical Research*, *106*, 18219−18238.

Kahn, R., Banerjee, P., McDonald, D., & Diner, D. (1998). Sensitivity of multiangle imaging to aerosol optical depth and a pure size distribution and composition over ocean. *Journal of Geophysical Research*, *103*, 32195−32213.

Kahn, R., Gaitley, B. J., Martonchik, J., Diner, D. J., & Crean, K. A. (2005). MISR global aerosol optical depth validation based on two years of coincident AERONET observations. *Journal of Geophysical Research*, *110*, doi:10.1029/2004JD004706

Kahn, R., West, R., McDonald, D., Rheingans, B., & Mishchenko, M. (1997). Sensitivity of multiangle remote sensing observations to aerosol sphericity. *Journal of Geophysical Research*, *102*, 16861−16870.

Krotkov, N. A., Bhartia, P. K., Herman, J. R., Fioletov, V., & Kerr, J. (1998). Satellite estimation of spectral surface UV irradiance in the presence of tropospheric aerosols 1. Cloud-free case. *Journal of Geophysical Research*, *103*, 8779−8793.

Kylling, A., Bais, A., Blumthaler, M., Schreder, J., Zerefos, C., & Kosmidis, E. (1998). Effect of aerosols on solar UV irradiancies during the photochemical activity and solar ultraviolet radiation campaign. *Journal of Geophysical Research*, *103*, 26051−26060.

Liley, J. B., & McKenzie, R. L. (1997, August). *Time-dependent wavelength non-linearities in spectrometers for solar UV monitoring* (pp. 845−848).

Lui, S., McKeen, S., & Mandronich, S. (1991). Effect of anthropogenic aerosols on biologically active ultraviolet radiation. *Geophysical Research Letters*, *18*, 2265−2268.

Madronich, S., McKenzie, R., Bjorn, L., & Caldwell, M. (1998). Changes in biologically active ultraviolet radiation reaching the Earth's surface. *Photochemestry and Photobiology*, *46*, 5−19.

Mayer, B., & Kylling, A. (2005). Technical note: The LibRadtran software package for radiative transfer calculations — description and examples of use. *Atmospheric Chemistry and Physics*, *5*, 1855−1877.

Mayer, B., Seckmeyer, G., & Kylling, A. (2004). Systematic long-term comparison of spectral UV measurements and UVSPEC modeling results. *Journal of Geophysical Research*, *102*, 8755−8767.

Middleton, N. J. (1984). Dust storms in Australia: Frequency, distribution and seasonality. *Search*, *15*, 46−47.

Mitchell, R. M., & Forgan, B. W. (2003). Aerosol measurement in the Australian outback: Intercomparison of sun photometers. *Journal of Atmospheric and Oceanic Technology*, *20*, 54−66.

O'Brien, D. M., & Mitchell, R. M. (2003). Atmospheric heating due to carbonaceous aerosol in northern Australia — confidence limits based on toms aerosol index and sun-photometer data. *Atmospheric Research*, *66*, 21−41.

Prospero, J. M., Ginoux, P., Torres, O., Nicholson, S. E., & Gill, T. E. (2002). Environmental characterization of global sources of atmospheric soil dust identified with the NIMBUS 7 Total Ozone Mapping Spectrometer (TOMS) absorbing aerosol product. *Reviews of Geophysics*, *40*(1), doi:10.1029/2000RG000095

Salomonson, V., Barnes, W. L., Xiong, X., Kempler, S., & Masuoka, E. (2002). An Overview of the Earth Observing System MODIS Instrument and Associated Data Systems Performance. *Proceedings of the international geoscience and remote sensing symposium IGARSS 02, Sydney, Australia*.

Shao, Y., & Leslie, L. (1997). Wind erosion prediction over the Australian continent. *Journal of Geophysical Research*, *102*, 30091−30106.

Slevin, T., Clarkson, J., & English, D. (2000). Skin cancer control in Western Australia: Is it working and what have we learned? *Radiation Protection Dosimetry*, *91*, 303−306.

Sqires, V.R., 2004. Dust and sandstorms: An early warning of impending disaster. *Dust and Sandstorms from the World's Drylands Part I- Physics, Mechanics and Processes of Dust and Sandstorms*, http://www.unccd.int/publicinfo/duststorms/menu.php

Stamnes, K., Tsay, S. C., Wiscombe, W., & Jayaweera, K. (1988). Numerically stable algorithm for discrete-ordinate-method radiative transfer in multiple scattering and emitting layered media. *Applied Optics*, *27*, 2502−2509.

Torres, O., Bhartia, P. K., Hermann, J. R., Ahmad, Z., & Gleason, J. (1998). Derivation of aerosol properties from satellite measurements of backscattering ultraviolet radiation: Theoretical basis. *Journal of Geophysical Research*, *103*, 17099−17110.

VanHoosier, M. E. (1996). Solar ultraviolet spectral irradiance with increased wavelength and irradiance accuracy. *SPIE Proceedings*, *2831*, 57−64.

Weihs, P., & Webb, A. R. (1997). Accuracy of spectral UV model calculations 1. Consideration of uncertainties in input parameters. *Journal of Geophysical Research*, *102*, 1541−1550.

WHO (2002). *Global solar UV index: A practical guide.* Geneva: World Health Organization.

Wuttke, S., Seckmeyer, G., Bernhard, G., Ehramjian, J., McKenzie, R., Johnston, P., et al. (2006). New spectroradiometers complying with the NDSC standards. *Journal of Atmospheric and Oceanic Technology*, *23*, 241−251.

Zeng, J., McKenzie, R., Stamnes, K., Wineland, M., & Rosen, J. (1994). Measured UV spectra compared with discrete ordinate method simulations. *Journal of Geophysical Research*, *99*, 23019−23030.